# Model-Free Subsurface Anomaly Detection using Subspace Analysis Techniques for Sparse Telemetry for Extraterrestrial Drilling Robots

Sarah Boelter[1], Greta Brown[1], Ebasa Temesgen[1], Lucas Weber[2], Thomas Stucky[3], Brian Glass[4], Maria Gini[1]

***Abstract*— In extraterrestrial planetary environments, computing, energy, and environmental constraints require robotic agents to complete tasks unsupervised. For specialized extraterrestrial robotic drilling agents there is no broadly applicable solution to detect drilling faults as they happen, before the fault escalates to hardware failure. We build upon previous work with time-series subspace analysis methods to to estimate drilling faults using drill avionics telemetry. This work introduces a subsurface anomaly detection method for planetary drilling robots and further evaluates the robustness of our time-series subspace analysis method. We implemented this novel fault and anomaly detection method on an extraterrestrial drilling robot and evaluated it first in a controlled lab environment with composite materials and then in a Mars planetary analog site in the Canadian High Arctic.**

## I. Introduction

This paper focuses on an extraterrestrial robotic drill , known as "The Regolith and Ice Drill for Exploring New Terrain" (TRIDENT) [1], shown in Figure 1 on a lander field test in Spain. It is a 1-meter rotary percussive drill manufactured by Honeybee Robotics. Despite several years of field and lab testing, we still only have relatively few instances of drilling fault data. The robotic drill gives indicators, visually or audibly, of a drilling fault well before it happens. Even with telemetry indicators, the ability to detect subsurface faults and anomalies is still missing, and the lack of training data makes training conventional supervised machine learning models difficult.

In this work, we build upon our previous research with subspace analysis techniques [2], which evaluated the accuracy of subspace analysis method, Enhanced Singular Spectrum Transformation (ESST), against other Change Point Detection (CPD) methods for fault and anomaly detection on robotic drills. The major contributions of this work are:

- A subsurface fault and anomaly detection method using avionics telemetry from extraterrestrial robotic drills, effective in environments requiring autonomy, based on the subspace analysis method, ESST.
- Evaluation of our subsurface fault and anomaly detection method on a robotic drilling system in a lab environment with regolith simulant materials.
- Evaluation of our subsurface fault and anomaly detection method on the same robotic drilling system in a Mars analog field environment [3] at Haughton Crater in the Canadian High Arctic.

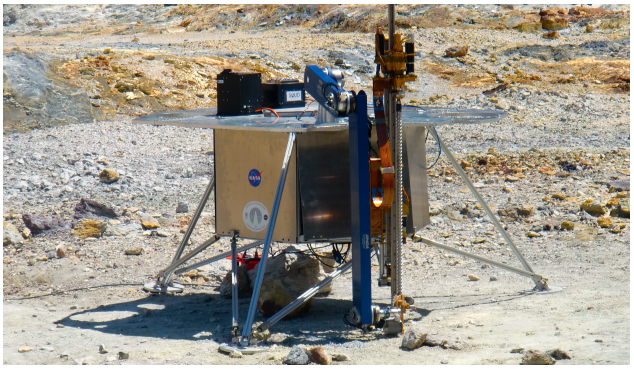

Fig. 1. Robotic drill lander concept in Spain in 2017

## II. Project Background

The Atacama Rover Astrobiology Drilling Studies (ARADS) project aimed to explore and understand the distribution of biosignatures, and extant life down to a one meter depth in planetary environments using a rover with an attached drill. This system was tested in Chile in September 2019. Diagnostic and automation software, IceBreaker Executive (IbExec), was prototyped [1], [4]. At the core of IbExec is the Plan Execution and Interchange Language (PLEXIL), a synchronous reactive language enabling control of the extensible hardware interface.

Figure 2 shows time-series from two boreholes. The first shows a normal drilling operation, the second illustrates a fault. Faults tend to raise variables like motor torque $\tau$ (the force applied by the motor) while the rate of penetration (ROP) $\rho$ (drill string velocity relative to the y-axis) is roughly zero. Other monitored sensor data include acoustic data and geophone data to better understand the subsurface before drilling [5].

## III. Related Work

### A. Autonomy in Extraterrestrial Subsurface Environments

Autonomy in extraterrestrial environments remains challenging. The 1997 Sojourner mission relied on Earth-based control, straining ground crews and highlighting the need for

[1]Department of Computer Science and Engineering, University of Minnesota Twin-Cities, Minneapolis, Minnesota 55416, USA {boelt072, brow6802, temes021, gini}@umn.edu

[2]Friedrich-Alexander-Universität Erlangen-Nürnberg, Germany 91058 {lucas.weber}@fau.de

[3]KBR Wyle Serives LLC, Moffett Field, California 94043, USA {thomas.stucky}@nasa.gov

[4]NASA Ames Research Center, Moffett Field, California 94043, USA {brian.glass}@nasa.gov

This work is supported by the Minnesota Space Grant Consortium, NASA PSTAR Mars Exploring through Analog-site Drilling (MEAD), and National Science Foundation CSGrad4US Fellowship under Grant No. 2240197.

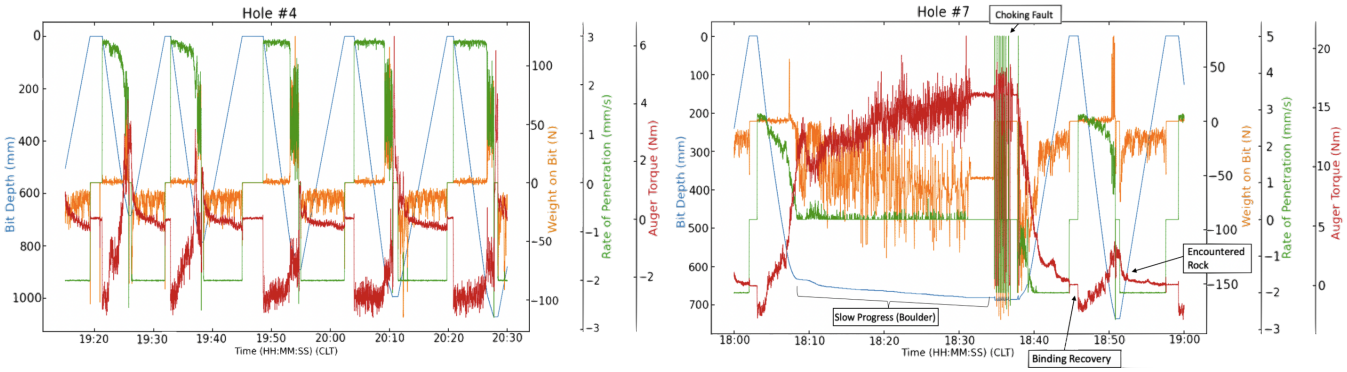


Fig. 2. Time series data showing Depth, Weight on Bit, Rate of Penetration, and Auger Torque throughout drilling 10 cm incremental bites in Devon Island, Canada. The left image shows normal drilling operations. The right image illustrates a choking fault where the Torque and Weight on Bit spike.

onboard autonomy [6]. The heavy Soviet Luna 16, 20, and 24 landers of the 1970s could drill up to 2 meters due to their mass, unlike modern ∼200 kg rovers [7]. This has driven research into lightweight drilling systems [1]. Autonomy in planetary drilling requires adapting reinforcement learning and control methods. Statham [8] used Structural Health Monitoring (SHM) to track vibrational frequencies of the DAME drill [9] for online assessment of ambient excitations. These methods are less effective on percussive drills. Tang et al. [10] propose a real-time drilling strategy using Support Vector Machines (SVMs) based on rate of penetration (RoP), but limited seismic data hinders model tuning in planetary environments and require training data. Extraterrestrial subsurface node-based technologies [11] offer means to map geophysical subsurface properties, but require human assistance. Other methods to explore planetary subsurface include burrowing robots [12] and Exobiology Extant Life Surveyor (EELS), a snake-like robot for exploring vents on Saturn's moons [13].

### B. State Estimation in Drilling

The Norwegian Research Center's taxonomy [14] notes that due to complexity, uncertainty, and limited subsurface observability, automation from other industries may not suit planetary drilling. Estimating the drilling system's internal state is essential. NORCE developed a method using a Markov Decision Process and Reinforcement Learning to optimize drilling [15]. Autonomous methods have been applied in surface and subsurface mining [16]. Sandia National Lab [17], [18] explores autonomy for pneumatically controlled percussive drilling through known layers using classification and Detournay-based optimization. Autonomous drilling is also used in domains with limited human presence or high precision, such as scientific fieldwork [19].

### C. Change Point Detection and Signal Segmentation

Time series CPD algorithms have a broad range of applications [20], [21], [22], [23], [24]. They aim to find discrete points where signals change to identify when the generating process has changed. For our use case, we have the following requirements:

1) Online Detection: To process and detect incoming data online to catch fault indications.
2) Unsupervised: Datasets are few and difficult to obtain, therefore, training supervised models is out of scope.
3) Data Efficiency: Drilling is unobservable and unpredictable needing methods requiring little calibration.
4) Computational Efficiency: Limited computational resources require efficient algorithms.
5) Robust: Data are noisy due to percussion and other effects, requiring a robust parameter-free method.

Since we require online, unsupervised detection, we exclude methods like Binary Segmentation, supervised approaches [21], and computationally intensive algorithms like TIRE [25]. Time series segmentation methods such as FLOSS [26] and ClaSP [22] were viable, but did not perform well when tested on datasets [2]. FLOSS detects change points using matrix profiles and nearest neighbor crossings, while ClaSP trains a binary classifier to distinguish segments before and after a potential change. Subspace methods, based on SSA, decompose the time series and compare subsequence shapes to detect changes [27], [28], [29], [30].

## IV. Methods

### A. Subspace-based Change Point Detection

Subspace-based CPD methods are best suited for detecting instantaneous morphological changes without requiring extensive historical sequences. They do not extract statistical properties but mainly characteristic shapes, and ignore noise, as the decomposition acts as a filter for random signal contributions. While noise filtering can be a disadvantage for statistical CPD [31], and the lack of "long-term memory" reduces their usability for segmentation, we believe they are promising for the unique properties and requirements of our application scenario (see sec. III-C). Subspace-based CPD methods use the SVD of two trajectory matrices $H_i$ and $H_j$ with $i < t < j$ to extract representative sequences before and after $(+\delta t)$ some point in time $t$ and compare them to provide a change point score [28], [29], [27].

The SVD of an arbitrary matrix returns three matrices $\text{SVD}(H_t) = U_t \Sigma_t V_t^T$, where the columns of $U_t$ contain the

left singular vectors, $\Sigma_t$ the singular values in decreasing order on the main diagonal, and $V_t$ the right singular vectors. Applied to time-series trajectory matrices, the right singular vectors $U_t$ can be seen as characteristic time series, while the corresponding right singular vectors quantify how well these characteristics represent each original time-series subsequence (columns of the trajectory matrix) individually, and the corresponding singular values quantify how well they represent the original time-series subsequences overall. Truncating the matrices to only $k$-major vectors represents the best rank-$k$ approximation of the time series subsequences contained in $H_t$ for the $l_2$ and Frobenius norm [32]. In other words, if one had to choose only $k$ time series characteristics, the major singular vectors would suit best in terms of the quadratic norm [2]. For subspace-based CPD, the Singular Spectrum Transformation (SST) [29], [33] is a well-used method. It evaluates a time series for changes by comparing the extracted characteristics at two different points in time ($t$ and $t + \delta t$):

$$S_T^t = 1 - ||(U_{t,k})^T U_{t+\delta t}^0||^2 = 1 - \sum_{i=0}^{k-1} \left((U_t^i)^T U_{t+\delta t}^0\right)^2 \quad (1)$$

where $U_{t,k}$ contains the top $k$ left singular vectors of the trajectory matrix $H_t$, $U_t^i$ denotes the $i^{\text{th}}$ left singular vector, and $U_{t+\delta t}^0$ contains the major right singular vector of time series subsequences extracted at a later point in time ($t+\delta t$). A low score indicates similarity (no change), while a high score signals a change point.

Earlier research demonstrated that ESST, a modified SST version, outperforms SST and other methods for the noisy signals encountered for robotic drills [2]. Unlike its competitors, ESST embeds both past and future subsequences into a single matrix and extracts the score by analyzing whether there are major characteristics that are only present in either past (at time $t$) or future subsequences (at time $t + \delta t$). With that, we can incorporate more information from the future subsequences into our final change score. Mathematically, we analyze the $k$-major right singular vectors $V_k$ of our two-sided trajectory matrix, where the first half of the columns are time series subsequences from time $t$, and the second half are time series subsequences around time $t + \delta t$:

$$\tilde{S}_T^t = \frac{\sum_{i=0}^{k-1} \sigma_i \left| \frac{1}{N} \left( \sum_{j=0}^{n/2-1} V^{i,j} - \sum_{j=n/2}^{n-1} V^{i,j} \right) \right|}{\sum_{i=0}^{k-1} \sigma_i}. \quad (2)$$

The ESST method has several parameters similar to SST: the rank $k$ of the subspace, essentially how many representative sequences are to be extracted; the number of sequences $n$, and the length $w$ of the subsequences that make up the trajectory matrices, which are $\delta t$ apart. The SST authors recommend only setting $w$ and keeping $n = w$. They also fix $\delta t = w/3$ to a third of the window size and fix $k = 5$ (low rank assumption). We keep these heuristics for ESST.

### B. Methods of Evaluation

The CPD algorithm evaluation lacks standardization and generalizability, with as many evaluation methods as algorithms. Benchmarks exist [34], but often lack noisy real-world sensor data. We chose methods suited to our application's specific constraints and evaluated them accordingly.

*1) F1 Score:* Fault rarity limit our evaluation options. CPD is often framed as a binary classification task: change or no change [21], [34], [20]. While prior work evaluates discrete change points, we assess performance per sample, resulting in a highly imbalanced dataset dominated by the no-change class. Since labeling all samples as "no change" yields high accuracy, we instead use F1-score to emphasize precision and recall for the minority (change) class. This aligns with evaluation methods in time series anomaly detection [35], where positive examples are similarly sparse.

*2) Standardized Mean Difference:* The Standardized Mean Difference (SMD) is a statistical measure used to quantify the magnitude of difference between two groups [36]. It is commonly applied in meta-analyses to facilitate comparisons across studies employing different tools, units, or methodologies. This makes it particularly suitable for our use case, where telemetry data and performance scores vary in scale and units, and the properties of the drilling material are unknown. We employ Cohen's *D*, a widely used form of SMD that utilizes the pooled standard deviation to calculate a *D* value. For reference, a *D* value of $\pm 0.2$ indicates a small difference between datasets, while a value of $\pm 0.8$ or higher suggests a large difference.

## V. Problem Formulation

Faults often manifest as sudden increases in motor torque $\tau$ or stalled penetration rates $\rho$, all of which is noisy data. We frame our problem as online CPD problem, formulated in three layers: signal, detection, and operational. At the signal layer, telemetry is streamed at $f_s = 40$ Hz, and can be decomposed into the following representation:

$$\mathbf{x}(t) = \begin{bmatrix} x^{(\tau)}(t) \\ x^{(\rho)}(t) \\ x^{(\alpha)}(t) \end{bmatrix} \in \mathbb{R}^3, \quad (3)$$

where $x^{(\tau)}(t)$ denotes the motor torque, $x^{(\rho)}(t)$ the rate of penetration (ROP), and $x^{(\alpha)}(t)$ the acoustic measurement at time $t$. Each channel is normalized online using a sliding window buffer $B$:

$$\tilde{x}^{(c)}(t) = \frac{x^{(c)}(t) - \mu_B^{(c)}}{\sigma_B^{(c)} + \epsilon}, \quad c \in \{\tau, \rho, \alpha\}. \quad (4)$$

Sliding windows of length $w$ are embedded into trajectory matrices $\mathbf{H}_t$, decomposed via truncated SVD. For channel $c$, the ESST change score is using eq. 2 where $\overline{v}_{i,\text{past}}^{(c)}$ and $\overline{v}_{i,\text{fut}}^{(c)}$ are means of the first and second halves of the right singular vector $\mathbf{v}_i$. The fused score across channels is:

$$S_t = \sum_{c \in \{\tau,\rho,\alpha\}} w_c \, S_t^{(c)}, \quad w_c \geq 0, \; \sum_c w_c = 1. \quad (5)$$

To bridge raw telemetry and fault threshold, we augment the signal representation with ESST-derived change scores. An anomaly score $S_t$ is computed and a binary alarm is raised whenever this score exceeds a pre-defined threshold

$\theta$, with threshold $\theta$ and hysteresis $L_{\min}$ to suppress chatter. For a true fault onset at time $t^\star$, the detection delay is:

$$\tau_{\text{detect}} = \min\{\Delta t \geq 0 : S_{t^\star+\Delta t} \geq \theta\}. \quad (6)$$

At the operational level, drilling efficiency depends on nominal operation plus additional time required for fault detection and mitigation. Let $T_{\text{nominal}}$ denote the expected drilling time with no faults, $F$ the set of possible faults, $P(f)$ the probability of a fault $f \in F$, $\tau_{\text{detect}}(f)$ the mean ESST detection delay, and $\tau_{\text{mitigate}}(f)$ the mean time to mitigate the fault. The expected total drilling time is therefore:

$$\mathbb{E}[T_{\text{drill}}] = T_{\text{nominal}} + \sum_{f\in F} P(f)\left(\tau_{\text{detect}}(f) + \tau_{\text{mitigate}}(f)\right). \quad (7)$$

Reducing detection delay $\tau_{\text{detect}}(f)$ decreases the expected drilling time, highlighting the operational value of ESST.

## VI. Experiments

### A. Lab Testing Experiments

*1) Implementation on Drill Hardware:* The ESST fault detection algorithm had been tested on the TRIDENT drill using recorded telemetry [2]. When integrating ESST with the drill avionics via PLEXIL at 40 Hz, we faced a trade-off between lower-rate sampling with data gaps and higher-rate sampling with potential duplicates. Due to planetary computational constraints, we chose lower-rate sampling and validated ESST with skipped time steps. As shown in Figure 3, the drill avionics pass motor telemetry to the PLEXIL Executive, which sends incremental data windows to the ESST Module. These windows are decomposed into trajectory matrices, and the right singular vectors are used to detect significant changes and compute a score. This score is then passed to the user for evaluation.

*2) Method Validation:* Testing before field deployment was done using composite materials designed to trigger faulty conditions, setup shown in Figure 4. It is important to understand the types of faults encountered in the drilling process in order to create materials to simulate those conditions. We took mixtures of cement, concrete, sand at different ratios along with additives like smooth granite at different layers to create our mixtures. Bucket types can be found in Table I. Mixtures were poured into buckets allowing 40 cm of drilling depth. Examples of faults are in Table II.

*3) Pre-Field Roverscape Validation:* After completing our implementation and conditional testing of the method against simulated faults, we tested the full setup for field conditions at our lab Roverscape, shown in Figure 4 to ensure methods worked with existing field workflow and other simultaneously used hardware without interference.

### B. Planetary Analog Field Site Experiments

*1) Field Site Evaluation and Testing:* The Haughton Impact Structure, a 23 km-wide crater on Devon Island, Nunavut, Canada, is a well-studied Mars analog site [37]. Its cold, dry environment closely resembling Martian surface conditions and ideal for testing space technologies. Features like frost polygonal terrain commonly seen in Martian high-

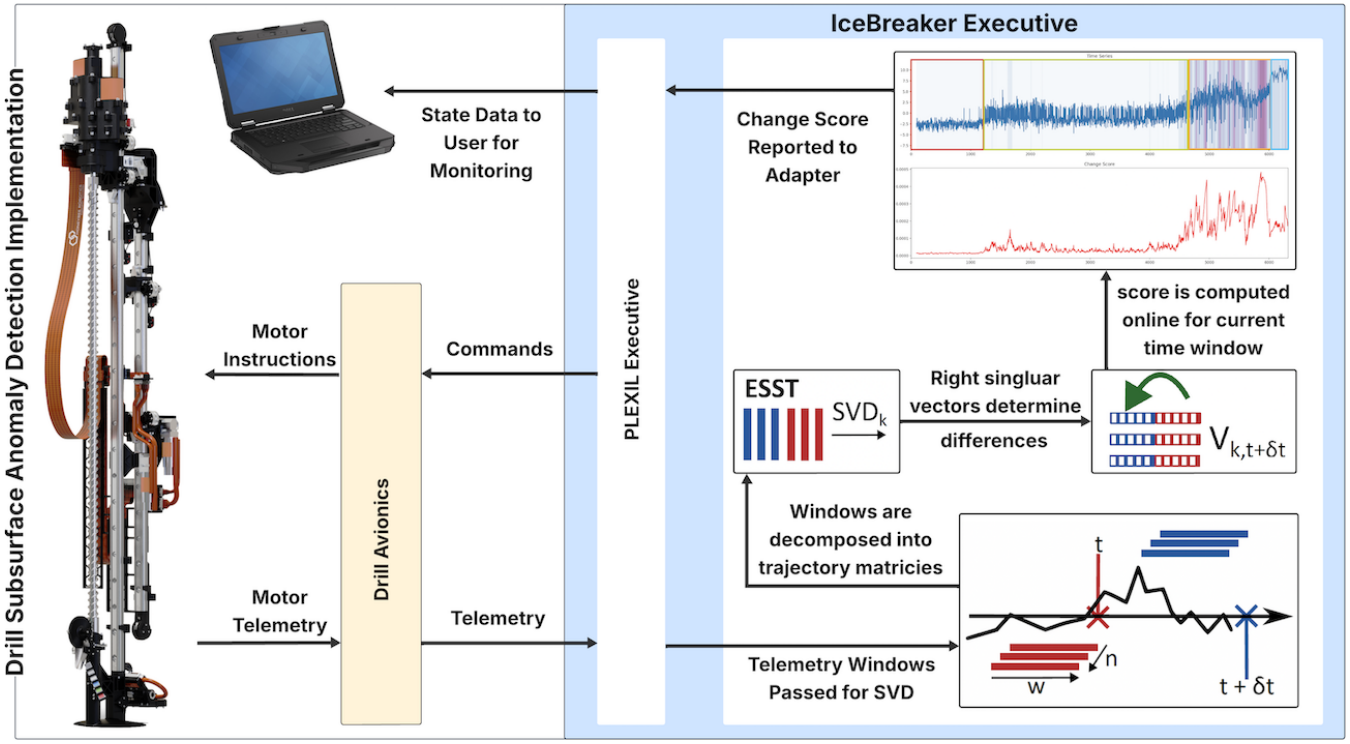


Fig. 3. Drill Subsurface Anomaly Detection Implementation. Motor Telemetry comes into the drill avionics. It is fed to the PLEXIL executive at a rate of 40Hz, and passes windows of data to our ESST Module. The data windows are then decomposed into trajectory matrices, and the right singular vectors determine any significant changes, which are then used to compute the score. The change score for the window is then passed to the user.

TABLE I

SIMULANT BUCKET FORMULATION FOR EXPERIMENTS

| Bucket Type | Ratios |
|---|---|
| 60:40 Sand:Concrete | Used as baseline and to test hardware functionality after faults, easy to drill |
| 80:20 Concrete:Sand | Used to induce bit inclusion and corkscrew faults. The gravely nature of the concrete will catch on bit |
| 80:20 Cement:Sand | Used to simulate choking and binding faults. Low porosity of cement leaves limited space for cuttings to disperse |
| 60:40 Cement:Sand w/ granite slabs | Used to induce hard materials faults and binding faults from difficulty drilling granite. |

latitude imagery make it ideal for surface and subsurface exploration research [38], [39], [40]. It has hosted previous Mars analog drilling tests [9] [41].

*2) Experiments:* An interdisciplinary team selected drilling sites to reflect likely choices for a Mars lander or rover (setup in Figure 4). The first site featured hydrothermal minerals, patterned ground, and a stream-cut edge, with no drilling faults. The second, on a fallback breccia hill with gravel, showed patterned ground and three recorded faults.

TABLE II

FAULT TYPES FOR PLANETARY DRILLING [8]

| Fault Type | Description |
|---|---|
| Binding Fault | Increased $\tau$ to to friction on drill string |
| Choking Fault | Cuttings caught in borehole increasing $\tau$ |
| Hard-Materials Fault | Stalled $\rho$ with increased $\tau$ |
| Corkscrewing Fault | Flutes caught on protruding rock |
| Bit Inclusion | Gravel caught in drill flutes increasing $\tau$ |

## VII. RESULTS & DISCUSSION

For lab and field testing, we monitored the telemetry variables $\tau$, $\rho$, and $\alpha$ and their respective change scores.

### A. Lab Testing Experiments

Lab tests allowed monitoring of drill and telemetry in a structured environment. We encountered six faults. Results appear in first row of Figure 5 and the lab column of Table III. Upper right of Figure 5 shows $\tau$ and its change score. After percussion begins, the change score rises with $\tau$ due to increased cuttings or bit inclusion, often leading to fault if unaddressed. In this case, $\tau$ increased until a fault occurred.

*1) SMD:* After verifying timestamps when fault symptoms began, we labeled our timeseries data, checked our change scores from the ESST algorithm, and plotted in 5, and notated scores in Table III. All our datasets had a Cohen's D score greater than $\pm$ 0.8, indicating the faulty telemetry data had a significant difference from the non-faulty telemetry data, giving us the ability to classify faulty and non-faulty telemetry and scores based on where it falls on our distribution.

*2) F1 Score:* For the F1-Score, shown in Table III, the closer it is to 1, the higher the precision and recall. We desire scores above 0.6. Numbers are rounded to two significant digits. The change scores of $\tau$ score, $\rho$ score, and $\alpha$ score all scored approximately above 0.6, indicating an excellent true positive fault detection.

*3) Discussion:* We find that ESST as implemented reinforces the findings of previous work [2], indicating that online monitoring of telemetry using ESST only enhances the monitoring and detection of anomalies and faulty states in the lab, despite the limited amount of existing training and testing data, setting up a good foundation for fieldwork.

### B. Planetary Analog Field Site Experiments

We had five fault-free and three faulty drilling instances. Faults were identified offline using telemetry of $\tau$, $\rho$, and $\alpha$,

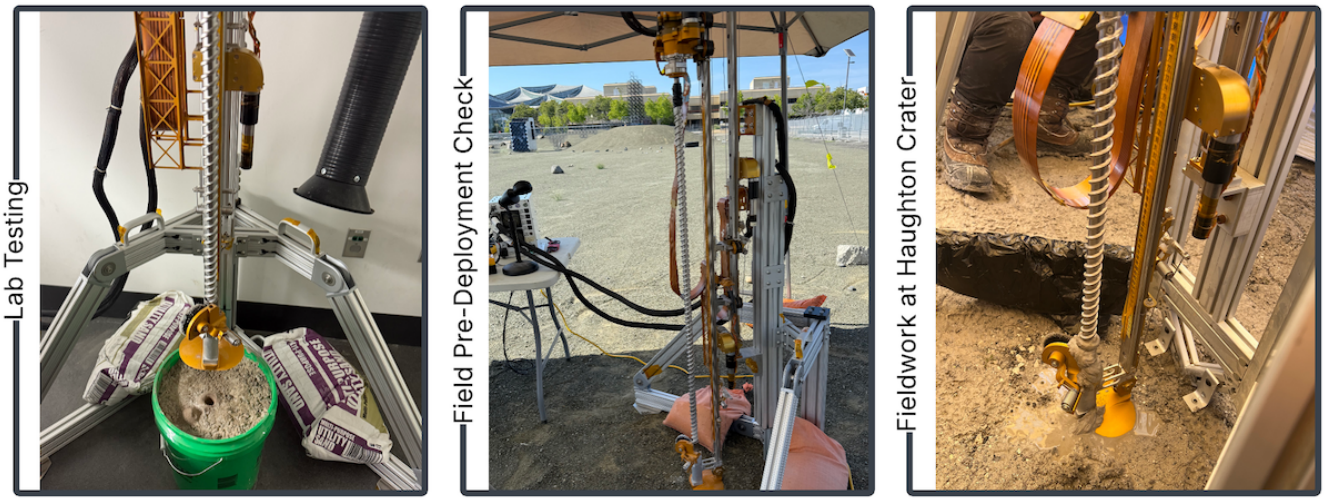


Fig. 4. Left is lab testing using regolith simulant buckets designed to quickly induce faults. Middle is pre-field deployment equipment validation at our lab roverscape, where software was tested in a mock-field setup ensuring proper setup before shipping gear to Haughton Crater. Right is drilling up to 1 m at Haughton Crater field site, testing fault and anomaly detection software in an environment mimicking mars conditions.

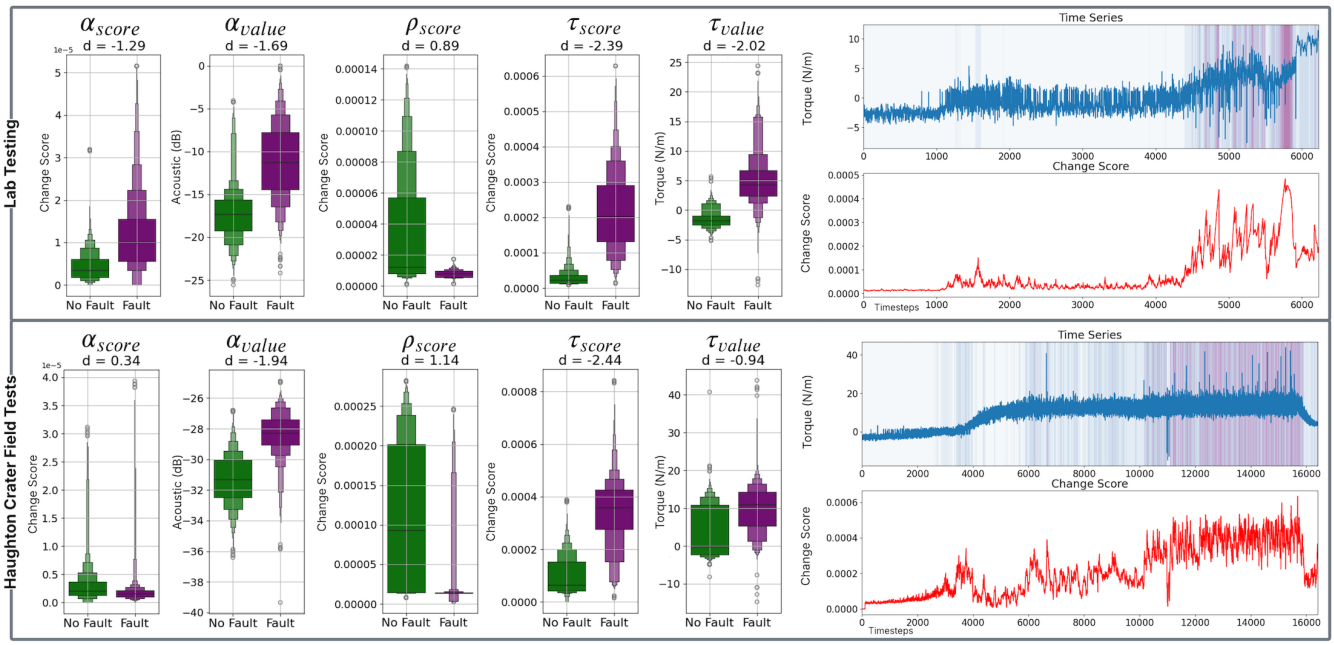


Fig. 5. Top set of graphs shows results from lab testing and bottom set of graphs results from Field testing. Left set of graphs in top and bottom show score distributions with and Cohen's D score showing the degree of difference between faulty and non-faulty datasets. Right top and bottom plots show motor torque $\tau$ time series data graphed over the course of a fault with the corresponding online change score. The top right was induced in the lab. The bottom right was a fault encountered at Haughton Crater Analog site. The purple shading indicates the severity of the change score, with the severity increasing with the buildup to the fault.

along with field notes on time, depth, and behavior. Field site results are shown in the second row of Figure 5. The lower right plot in Figure 3 shows a $\tau$ fault graph from the field, with progression similar to the lab example.

TABLE III
SMD COHEN'S D VALUE AND F1 SCORES FOR ALL RESULTS

| **Value** | **Dataset Cohen's D Value** | |
|---|---|---|
| **Location** | **Lab** | **Field Site** |
| $\tau$ value | -2.02 | -0.94 |
| $\tau$ score | -2.39 | -2.44 |
| $\rho$ score | 0.89 | 1.14 |
| $\alpha$ value | -1.41 | -1.94 |
| $\alpha$ score | -1.56 | 0.34 |
| **Value** | **Average F1 Score** | |
| **Location** | **Lab** | **Field Site** |
| $\tau$ score | 0.82 | 0.75 |
| $\rho$ score | 0.68 | 0.78 |
| $\alpha$ score | 0.60 | 0.54 |

*1) SMD:* We calculated SMD scores as we did for the lab testing. They are shown in Figure 5 and in Table III. All of our datasets except the $\alpha$ score had a Cohen's D score greater than $\pm 0.8$, indicating the faulty telemetry data for most of our datasets had a significant difference from our non-faulty telemetry data, reflecting lab results. Our $\alpha$ score dataset only had a small difference of $\pm 0.34$.

*2) F1 Score:* The F1-Scores are shown in Table III, and follow the same procedure as our lab experiments. For our field data, we evaluated the $\tau$ score, $\rho$ score, and $\alpha$ score. All of our lab datasets, except the $\alpha$ score, scored above 0.6, indicating good true positive recall.

*3) Discussion:* The $\alpha$ datasets likely differed much more than the controlled lab environment purely because of outdoor vs indoor environments having more wind and ambient noise, placement being difficult due to land features, etc. We believe the more favorable scores in the lab indicate acoustic methods for fault detection are a promising method in assisting with fault detection in planetary drilling, but for field environments, telemetry data from instruments are more resistant to ambient noise and placement. Additional instruments, such as a laser Doppler vibrometer or accelerometer, would yield more accurate results and open up avenues for future research directions. Otherwise, the results from $\rho$ score, $\tau$ score, and $\tau$ telemetry value indicate that our method for subsurface anomaly and fault detection is effective, even if the $\alpha$ telemetry value and change score did not have as clear an effect in field compared to the lab experiments.

## VIII. CONCLUSIONS AND FUTURE WORK

This work presented a subsurface fault and anomaly detection method using telemetry from TRIDENT and evaluated its effectiveness for fault detection in the lab and at a Mars-analog field site. We found our method effective for identifying faults and anomalies, allowing better incoming fault identification and detection. Future work involves incorporating anomaly detection into autonomous drilling methods.

## References


[1] B. Glass, D. Bergman, V. Parro, L. Kobayashi, C. Stoker, R. Quinn, A. Davila, P. Willis, W. Brinckerhoff, K. Warren-Rhodes, M. Wilhelm, L. Caceres, J. DiRuggiero, K. Zacny, M. Moreno-Paz, A. Dave, S. Seitz, A. Grubisic, M. Castillo, R. Bonaccorsi, and the ARADS Team, "The Atacama rover astrobiology drilling studies (ARADS) project."

[2] S. Boelter, L. Weber, R. Lenz, B. Glass, and M. Gini, "Fault prediction in drilling using subspace analysis techniques," *Intelligent Autonomous Systems 19, Proc. 19th Int'l Conf IAS-19*, 2025.

[3] "Analog Missions - NASA — nasa.gov," https://www.nasa.gov/analog-missions/, [Accessed 12-09-2025].

[4] S. Boelter, E. Temesgen, B. Glass, and M. Gini, "Understanding drill data for autonomous application," in *International Workshop on Autonomous Agents and Multi-Agent Systems for Space Applications at AAMAS*, 2024.

[5] C. Stoker, "Field tests with TRIDENT drill in Bishop Tuff help prepares for future missions to Moon and Mars," Universities Space Research Association, 2024.

[6] N. Muscettola, P. P. Nayak, B. Pell, and B. C. Williams, "Remote agent: to boldly go where no AI system has gone before," *Artificial Intelligence*, vol. 103, no. 1–2, pp. 5–47, 1998.

[7] G. Paulsen, K. Zacny, P. Chu, E. Mumm, K. Davis, S. Frader-Thompson, K. Petrich, D. Glaser, P. Bartlett, H. Cannon, and B. Glass, *Robotic Drill Systems for Planetary Exploration*. AIAA, 2006.

[8] S. M. Statham, "Autonomous structural health monitoring technique for interplanetary drilling applications using laser doppler velocimeters," Ph.D. dissertation, Georgia Institute of Technology, Atlanta, Georgia, 2011.

[9] B. Glass, H. Cannon, M. Branson, S. Hanagud, and G. Paulsen, "DAME: Planetary-prototype drilling automation," *Astrobiology*, vol. 8, pp. 653–64, 2008.

[10] J. Tang, Z. Deng, Q. Quan, and S. Jiang, "Real-time drilling strategy for planetary sampling: Method and validation," *Journal of Aerospace Engineering*, vol. 29, no. 5, p. 04016033, 2016.

[11] D. Colombo, E. Sandoval-Curiel, T. Alyousuf, E. Turkoglu, and D. Rovetta, "Ultra-dense nodal seismic acquisition for automated geohazard analysis," *The Leading Edge*, 2024.

[12] Y. Liu, Z. Yuan, Y. Li, and H. Zhao, "A Three-dimensional path planning method of autonomous burrowing robot for lunar subsurface exploration," in *2021 6th IEEE International Conference on Advanced Robotics and Mechatronics (ICARM)*, Jul. 2021, pp. 710–715. [Online]. Available: https://ieeexplore.ieee.org/document/9536059/

[13] T. S. Vaquero, G. Daddi, R. Thakker, M. Paton, A. Jasour, M. P. Strub, R. M. Swan, R. Royce, M. Gildner, P. Tosi, M. Veismann, P. Gavrilov, E. Marteau, J. Bowkett, D. L. de Mola Lemus, Y. Nakka, B. Hockman, A. Orekhov, T. D. Hasseler, C. Leake, B. Nuernberger, P. Proença, W. Reid, W. Talbot, N. Georgiev, T. Pailevanian, A. Archanian, E. Ambrose, J. Jasper, R. Etheredge, C. Roman, D. Levine, K. Otsu, S. Yearicks, H. Melikyan, R. R. Rieber, K. Carpenter, J. Nash, A. Jain, L. Shiraishi, M. Robinson, M. Travers, H. Choset, J. Burdick, A. Gardner, M. Cable, M. Ingham, and M. Ono, "EELS: Autonomous snake-like robot with task and motion planning capabilities for ice world exploration," *Science Robotics*, vol. 9, no. 88, p. eadh8332, Mar. 2024. [Online]. Available: https://www.science.org/doi/full/10.1126/scirobotics.adh8332

[14] J. Wardt, E. Cayeux, R. Mihai, J. Macpherson, P. Annaiyappa, and D. Pirovolou, "Taxonomy describing levels of autonomous drilling systems: Incorporating complexity, uncertainty, sparse data, with human interaction," in *IADC/SPE International Drilling Conference and Exhibition*, 2024.

[15] E. Cayeux, B. Daireaux, A. Ambrus, R. Mihai, and L. Carlsen, "Autonomous decision-making while drilling," *Energies*, vol. 14, p. 969, 2021.

[16] J. A. Marshall, "Mining robotics," *Encyclopedia of Robotics*, pp. 1–6, 2020.

[17] S. J. Spencer, A. Mazumdar, Jiann-Cherng Su, A. Foris, and S. P. Buerger, "Estimation and control for efficient autonomous drilling through layered materials," in *American Control Conference (ACC)*. Seattle, WA, USA: IEEE, May 2017, pp. 176–182. [Online]. Available: https://ieeexplore.ieee.org/document/7962950/

[18] A. Mazumdar, J.-C. Su, S. J. Spencer, and S. P. Buerger, "Autonomous control of pneumatically-powered percussive drilling through highly layered formations," in *American Control Conference (ACC)*. Philadelphia, PA, USA: IEEE, Jul. 2019, pp. 5215–5221. [Online]. Available: https://ieeexplore.ieee.org/document/8815280/

[19] C. Katlein, "Towards ice core sampling by subsea robotic vehicles," Nov. 2024. [Online]. Available: https://egusphere.copernicus.org/preprints/2024/egusphere-2024-3358/

[20] C. Truong, L. Oudre, and N. Vayatis, "Selective review of offline change point detection methods," *Signal Processing*, vol. 167, 2020.

[21] S. Aminikhanghahi and D. J. Cook, "A survey of methods for time series change point detection," *Knowl. Inf. Syst.*, vol. 51, no. 2, p. 339–367, 2017.

[22] A. Ermshaus, P. Schäfer, and U. Leser, "ClaSP: parameter-free time series segmentation," *Data Mining and Knowledge Discovery*, vol. 37, no. 3, pp. 1262–1300, 2023.

[23] A. Kazemi, "A semi-supervised approach to the application of sensor-based change- point detection for failure prediction in industrial instruments," Master's thesis, Norwegian University of Science and Technology (NTNU), 2019.

[24] L. Weber and R. Lenz, "Machine learning in sensor identification for industrial systems," *it - Information Technology*, vol. 65, no. 4-5, pp. 177–188, 2023.

[25] T. De Ryck, M. De Vos, and A. Bertrand, "Change point detection in time series data using autoencoders with a time-invariant representation," *IEEE Transactions on Signal Processing*, vol. 69, pp. 3513–3524, 2021.

[26] S. Gharghabi, Y. Ding, C.-C. M. Yeh, K. Kamgar, L. Ulanova, and E. Keogh, "Matrix Profile VIII: Domain agnostic online semantic segmentation at superhuman performance levels," in *Proceedings of the IEEE ICDM*, 2017, pp. 117–126.

[27] V. Moskvina and A. Zhigljavsky, "An algorithm based on singular spectrum analysis for change-point detection," *Communications in Statistics-Simulation and Computation*, vol. 32, pp. 319–352, 2003.

[28] T. Idé and K. Inoue, "Knowledge discovery from heterogeneous dynamic systems using change-point correlations," in *Proceedings of the SIAM International Conference on Data Mining*, 2005, pp. 571–575.

[29] T. Idé and K. Tsuda, "Change-point detection using Krylov subspace learning," in *Proceedings of the SIAM International Conference on Data Mining*, 2007, pp. 515–520.

[30] Y. Mohammad and T. Nishida, "On comparing SSA-based change point discovery algorithms," in *IEEE/SICE Int'l Symp. on System Integration*, 2011, pp. 938–945.

[31] S. Liu, M. Yamada, N. Collier, and M. Sugiyama, "Change-point detection in time-series data by relative density-ratio estimation," *Neural Networks*, vol. 43, 2013.

[32] C. Eckart and G. Young, "The approximation of one matrix by another of lower rank," *Psychometrika*, vol. 1, pp. 211–218, 1936.

[33] L. Weber and R. Lenz, "Accelerating singular spectrum transformation for scalable change point detection," *IEEE Access*, vol. 13, pp. 213 556–213 577, 2025.

[34] G. J. J. van den Burg and C. K. I. Williams, "An evaluation of change point detection algorithms," arXiv:2003.06222v3 [stat.ML], 2020.

[35] S. Schmidl, P. Wenig, and T. Papenbrock, "Anomaly detection in time series: A comprehensive evaluation," *Proceedings of VLDB Endowment*, vol. 15, no. 9, pp. 1779–1797, 2022.

[36] C. Andrade, "Mean difference, standardized mean difference (smd), and their use in meta-analysis: As simple as it gets," *The Journal of Clinical Psychiatry*, vol. 81, no. 5, p. 11349, 2020.

[37] G. R. Osinski, P. Lee, J. G. Spray, J. Parnell, D. S. S. Lim, T. E. Bunch, C. S. Cockell, and B. Glass, "Geological overview and cratering model for the Haughton impact structure, Devon Island, Canadian High Arctic," *Meteoritics & Planetary Science*, vol. 40, no. 12, pp. 1759–1776, 2005.

[38] T. D. Barfoot, P. T. Furgale, B. E. Stenning, P. J. F. Carle, J. P. Enright, and P. Lee, "Devon island as a proving ground for planetary rovers," in *Brain, Body and Machine*, J. Angeles, B. Boulet, J. J. Clark, J. Kövecses, and K. Siddiqi, Eds. Berlin, Heidelberg: Springer Berlin Heidelberg, 2010, pp. 269–281.

[39] P. Furgale, P. Carle, J. Enright, and T. D. Barfoot, "The Devon Island rover navigation dataset," *The International Journal of Robotics Research*, vol. 31, no. 6, pp. 707–713, May 2012. [Online]. Available: https://journals.sagepub.com/doi/10.1177/0278364911433135

[40] T. D. Barfoot, P. T. Furgale, G. R. Osinski, N. Ghafoor, and K. K. Williams, "Field testing of robotic technologies to support ground ice prospecting in martian polygonal terrain," *Planetary and Space*

*Science*, vol. 58, no. 4, pp. 671–681, Mar. 2010. [Online]. Available: https://linkinghub.elsevier.com/retrieve/pii/S0032063309002852

[41] B. J. Glass, A. Dave, C. P. McKay, and G. Paulsen, "Robotics and automation for "Icebreaker"," *Journal of Field Robotics*, vol. 31, no. 1, pp. 192–205, Jan. 2014. [Online]. Available: https://onlinelibrary.wiley.com/doi/10.1002/rob.21487